Electronic Supplementary Material (ESI) for New Journal of Chemistry.

Electronic Supplementary Information

Naphthoylhydrazones: coordination to metal ions and biological screening

*Nádia Ribeiro,[1] Adelino M. Galvão,[1] Clara S. B. Gomes,[1,2] Helena Ramos,[3] Rute Pinheiro,[3] Lucilia Saraiva, [3] Epole Ntungwe,[4] Vera Isca, [4,5] Patricia Rijo,[4,5] Isabel Cavaco,[1,6] Filipa Ramilo-Gomes,[1,7] Rita C. Guedes,[7] João Costa Pessoa,[1] Isabel Correia[1,]**

[1]*Centro de Química Estrutural, Instituto Superior Técnico, Universidade de Lisboa, Portugal*

[2]*LAQV-REQUIMTE, Departamento de Química, Faculdade de Ciências e Tecnologia, Universidade NOVA de Lisboa, 2829-516, Caparica, Portugal*

[3] *LAQV-REQUIMTE, Laboratório de Microbiologia, Departamento de Ciências Biológicas, Faculdade de Farmácia, Universidade do Porto, Porto, Portugal*

[4]*CBIOS - Research Center for Biosciences & Health Technologies, U. Lusófona de Humanidades e Tecnologias, Lisboa, Portugal*

[5]*Instituto de Investigação do Medicamento (iMed.ULisboa), Faculdade de Farmácia, Universidade de Lisboa, Lisboa, Portugal*

[6] *Departamento de Química Bioquímica e Farmácia, Universidade do Algarve, Campus de Gambelas, 8005-139 Faro, Portugal*

[7]*Instituto de Investigação do Medicamento (iMed.ULisboa), Faculdade de Farmácia, Universidade de Lisboa, Lisboa, Portugal*

ESI 1 - X-ray diffraction

The molecular structure of HL^2 was unambiguously determined by X-ray diffraction. An ORTEP diagram presenting one molecule of the asymmetric unit is depicted in Fig. 1, and selected bond lengths and angles are listed in Table S1.

Compound HL^2 crystallized as yellow prisms, in the monoclinic system, space group $P2_1/c$, showing three independent molecules in the asymmetric unit (Fig. S1).

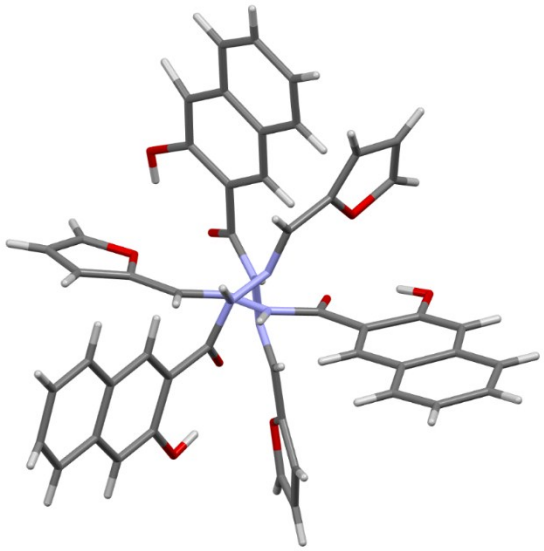

Figure S1 - Asymmetric unit of compound **HL^2**, viewed along *a*.

The structures of molecules A and B of the asymmetric unit display almost planar backbones, with angles between the planes of the naphthoyl substituent and the furan-hydrazide group of 11.15(10) and 13.97(11)º, respectively. On the other hand, for molecule C, this angle increases to 32.33(19)º. All distances and angles are within the expected values for similar compounds.[1]

The supramolecular arrangement of compound HL^2 is mainly generated by classic O–H···O, N–H···O and N–H···N hydrogen bonds, as depicted in Fig. S2 and described in Table S2.

Table S1 - Selected bond lengths (Å) and angles (º) for compound HL^2.

	HL^2		
	molecule A	*molecule B*	*molecule C*
Bond lengths (Å)			
C1–O1	1.362(4)	1.355(4)	1.321(4)
C1–C2	1.336(5)	1.335(5)	1.346(6)
C2–C3	1.431(6)	1.400(6)	1.384(6)
C3–C4	1.306(6)	1.306(6)	1.292(6)
C4–O1	1.359(5)	1.371(5)	1.375(5)
C1–C5	1.445(5)	1.430(5)	1.420(5)
C5–N1	1.265(4)	1.263(4)	1.258(4)
N1–N2	1.384(3)	1.385(3)	1.382(3)
N2–C6	1.335(3)	1.336(3)	1.345(3)
C6–O2	1.248(3)	1.248(3)	1.247(3)
C6–C7	1.478(4)	1.467(4)	1.476(4)
C8–O3	1.353(4)	1.336(4)	1.376(5)
Angles (°)			
O1–C1–C5	119.1(3)	119.4(3)	119.4(3)
C5–N1–N2	115.0(3)	115.5(2)	115.7(2)
C6–N2–N1	117.77(17)	117.96(18)	118.66(17)
O2–C6–N2	121.3(3)	121.3(3)	121.4(3)
N2–C6–C7	117.8(2)	118.2(3)	117.3(2)
O3–C8–C7	121.4(3)	121.9(3)	121.4(4)

Table S2 - List of hydrogen bonds for HL^2 [Å and °].

D-H...A	*d*(D-H)	*d*(H...A)	*d*(D...A)	<(DHA)
O3A-H30A...O2A^{i}	0.82	1.85	2.5767(9)	146
O3B-H30B...O2B^{ii}	0.82	1.80	2.5325(9)	147
O3C-H30C...O2C	0.82	1.93	2.6262(9)	142
N2A-H20A...O2C	1.06	1.96	2.9311(10)	152
N2A-H20A...N1C	1.06	2.55	3.3376(12)	131
N2B-H20B...O2A^{i}	1.03	2.02	2.9809(10)	154
N2B-H20B...N1A^{ii}	1.03	2.60	3.4067(12)	136
N2C-H20C...O2B	1.04	2.08	2.9231(10)	137
N2C-H20C...N1B	1.04	2.36	3.2909(11)	148

Symmetry transformations used to generate equivalent atoms:

^{i} *1-x,-1/2+y+1,1/2-z* ^{ii} *-x,1/2+y,1/2-z*

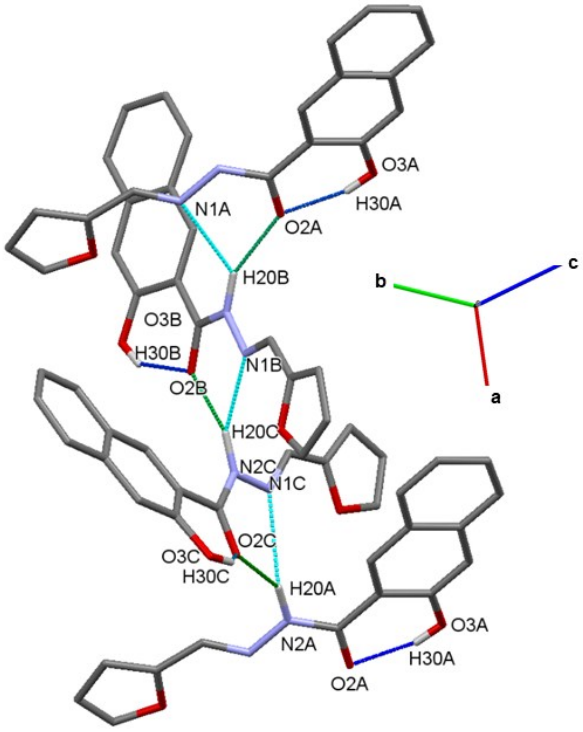

Figure S2 - View of the hydrogen bonds for compound HL^2. Donor and acceptor atoms are identified. Blue, light-blue and green dashed lines represent the O–H···O, N–H···N and N–H···O hydrogen bonds, respectively. All the hydrogen atoms, except those involved in the interactions, were omitted for clarity.

ESI2 – Calculated *vs.* experimental IR frequencies

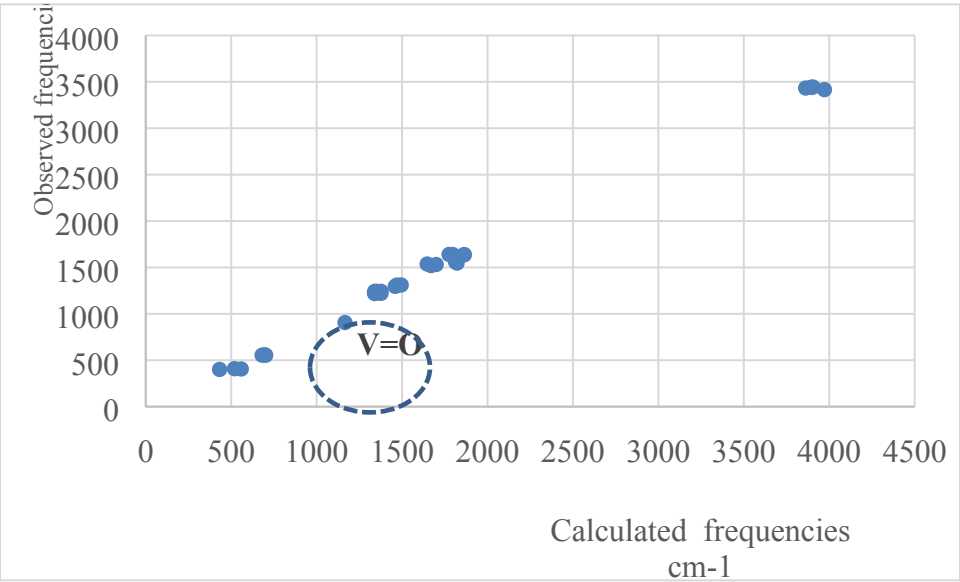

Figure S3 – Calculated *vs.* experimental IR frequencies (cm^{-1}) for HL^1, HL^3 and HL^2 derived complexes. The scale factor of 0.88 compares well with a value of 0.9 for the CPHF methodology at the NIST-**C**omputational **C**hemistry **C**omparison and **B**enchmark **D**ata**B**ase.

ESI 3 – Spectroscopic Characterization

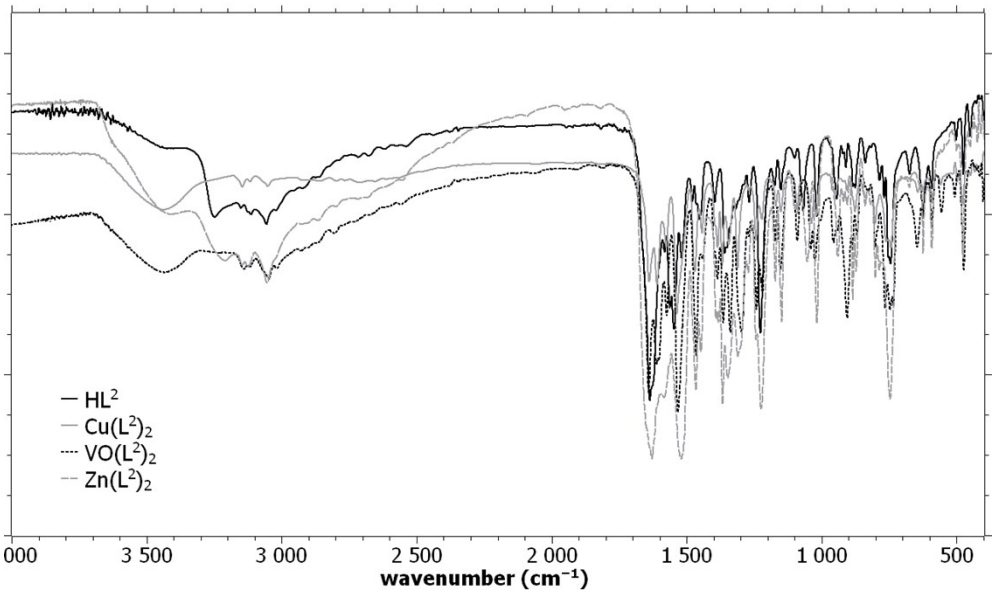

Figure S4 – Infra-red spectra of HL^2 and its Cu(II), VO(IV) and Zn(II) complexes obtained as KBr pellets.

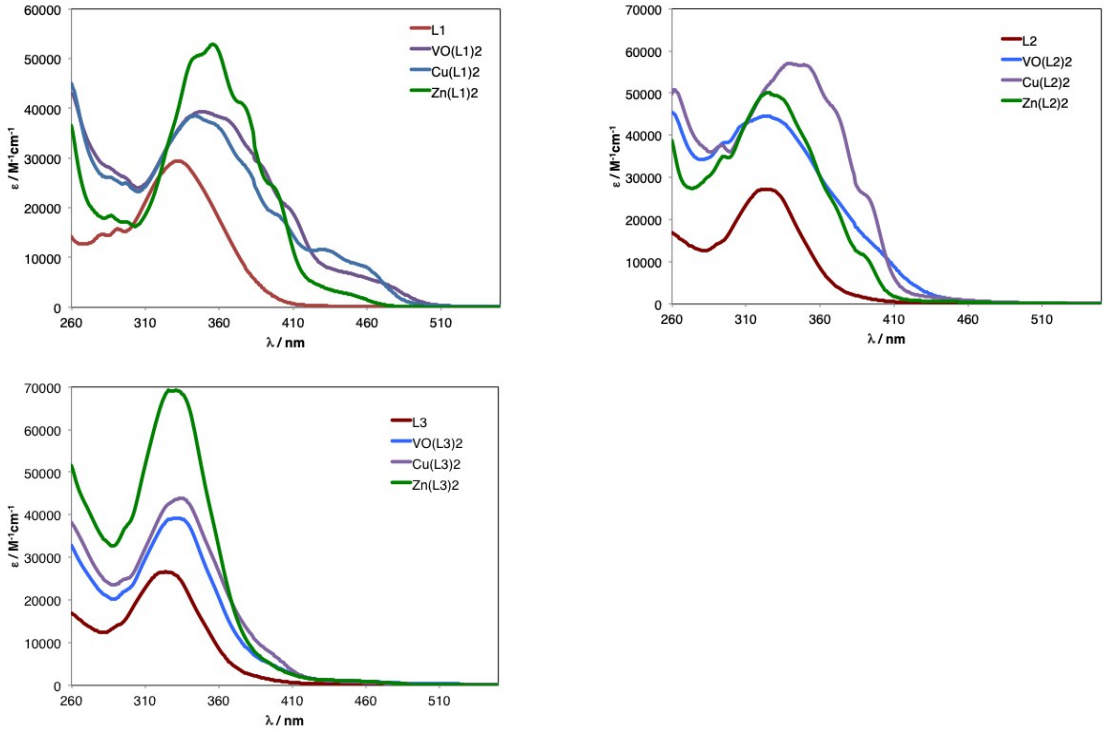

Figure S5 – UV-Vis spectra of the compounds in DMSO. Concentration *ca.* 20-30μM.

The ^{1}H NMR, ^{13}C NMR APT (Attached-Proton-Test), homonuclear Correlation Spectroscopy (^{1}H-^{1}H COSY), Heteronuclear Single Quantum Coherence (HSQC) and Heteronuclear Multiple Bonds Coherence (HMBC) were used to assign the NMR peaks to the ligands' atoms shown (Table S3).

Table S3 – Chemical shifts (ppm) in DMSO-d_6 using TMS as internal reference for proton and carbon atoms in HL^1, HL^2 and HL^3 structures using the labeling presented in the Figure below, as well as for the Zn-complexes.

	L^1		$Zn(L^1)_2$ (7)		L^2		$Zn(L^2)_2$ (8)[b]		L^3		$Zn(L^3)_2$ (9)	
	H	C	H	C	H	C	H	C	H	C	H	C
1	—	126.75	—	126.72	—	149.29	—	148.97	—	139.05	—	139.54
2	6.54	113.97	7.03	120.03	6.97	114.09	7.07	114.33	7.17	128.44	7.16	128.36
3	6.17	109.36	6.39	110.96	6.66	112.33	6.58	112.01	7.51	131.59	7.35	123.96
4	6.95	123.77	7.31	125.41	8.35	138.18	8.4	140.61	7.71	129.54	7.54	131.7
5	8.30	141.70	8.70	148.17	7.88	145.48	7.64	145.55	8.67	143.72	8.65	143.88
6	—	163.49	—	167.20	—	163.69	—	[a]	—	163.76	—	164.11
7	—	119.93	—	120.36	—	120.48	—	[a]	—	120.68	—	121
8	—	154.49	—	155.98	—	153.99	—	154.87	—	154.19	—	154.7
9	7.31	110.56	7.29	110.23	7.36	123.83	7.3	123.15	7.32	110.76	7.29	110.78
10	—	135.79	—	135.75	—	135.83	—	136.66	—	136.02	—	136.34
11	7.76	125.84	7.74	125.84	7.75	125.80	7.69	125.65	7.36	124.03	7.79	126
12	7.51	128.17	7.45	127.72	7.51	128.25	7.46	128.14	7.91	128.18	7.89	128.4
13	7.36	122.93	7.29	123.27	7.32	110.55	7.25	110	7.76	126.11	7.79	129.58
14	7.91	128.64	7.82	128.9	7.90	128.68	7.84	128.33	7.51	128.91	7.47	128.88
15	—	126.68	—	126.72	—	126.75	—	118.84	—	127.00	—	126.88
16	8.46	129.83	8.48	129.53	8.42	130.23	8.55	130	8.41	130.38	8.42	130.61
OH	11.48	—	13.34	—	11.92	—		—	11.25	—		—
NH	11.74	—	—	—	11.26	—		—	11.93	—		—
$NH_{pyrrole}$	11.61	—	12.6	—	—	—	—	—	—	—	—	—

[a] not detected within the concentrations used

[b] measured in MeOD

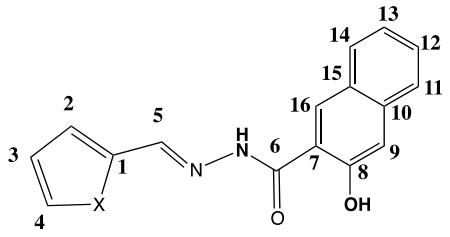

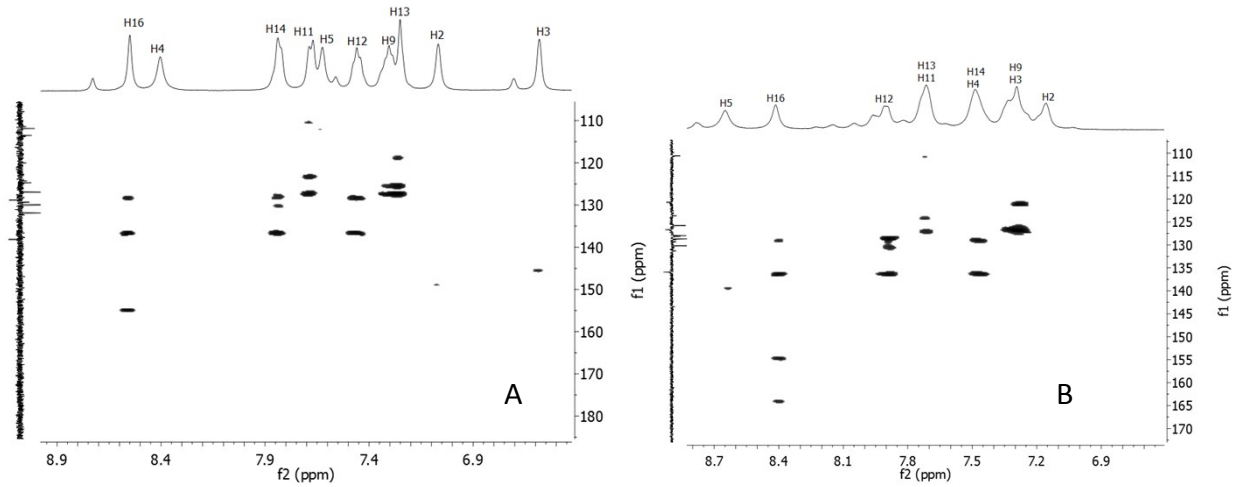

Figure S6 – A) HMBC correlation spectrum of $Zn(L^2)_2$, **8**, in MeOH-d_4 and B) HMBC correlation spectrum of $Zn(L^3)_2$, **9**, in DMSO-d_6. Chemical shifts in ppm using TMS as internal reference.

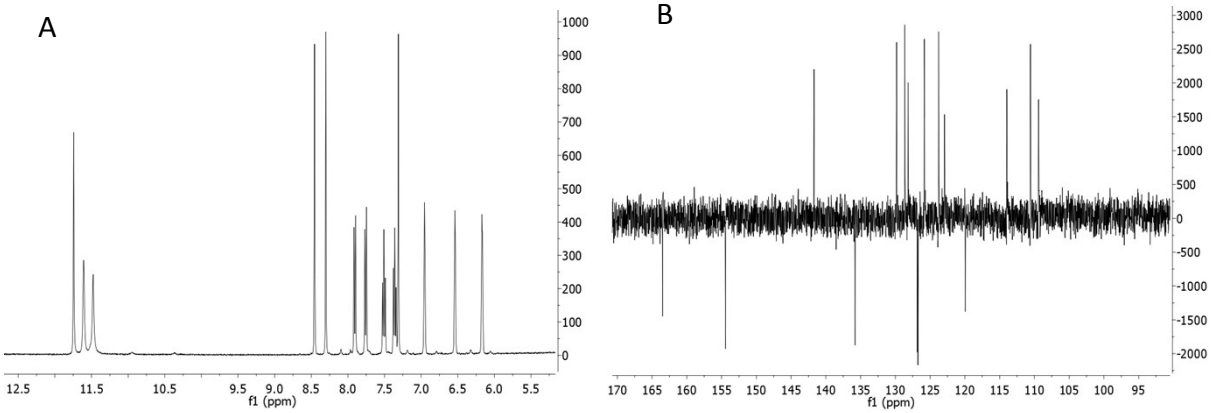

Figure S7 – ^{1}H NMR (A) and ^{13}C DEPT (Distortionless enhancement by polarization transfer) NMR (B) spectra of HL^1 in DMSO-d_6 (chemical shifts in ppm, using TMS as internal reference).

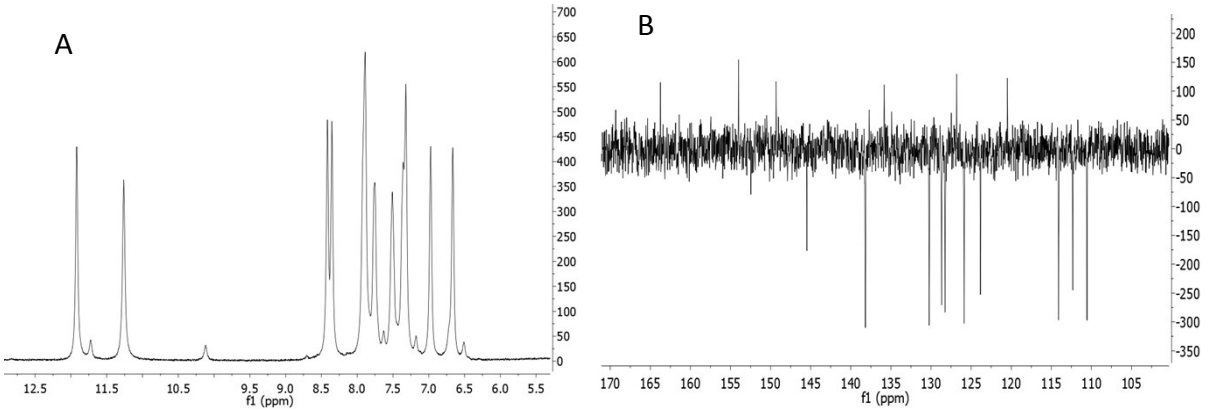

Figure S8 – ^{1}H NMR (A) and ^{13}C APT NMR (B) spectra of HL^2 in DMSO-d_6 (chemical shifts in ppm, using TMS as internal reference).

B

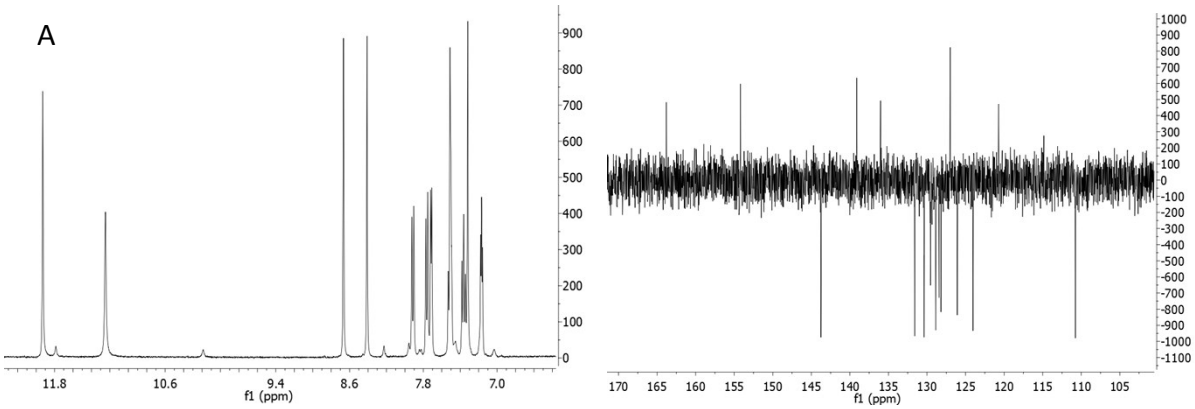

Figure S9 – ^{1}H NMR (A) and ^{13}C APT NMR (B) spectra of HL^3 in DMSO-d_6 (chemical shifts in ppm, using TMS as internal reference).

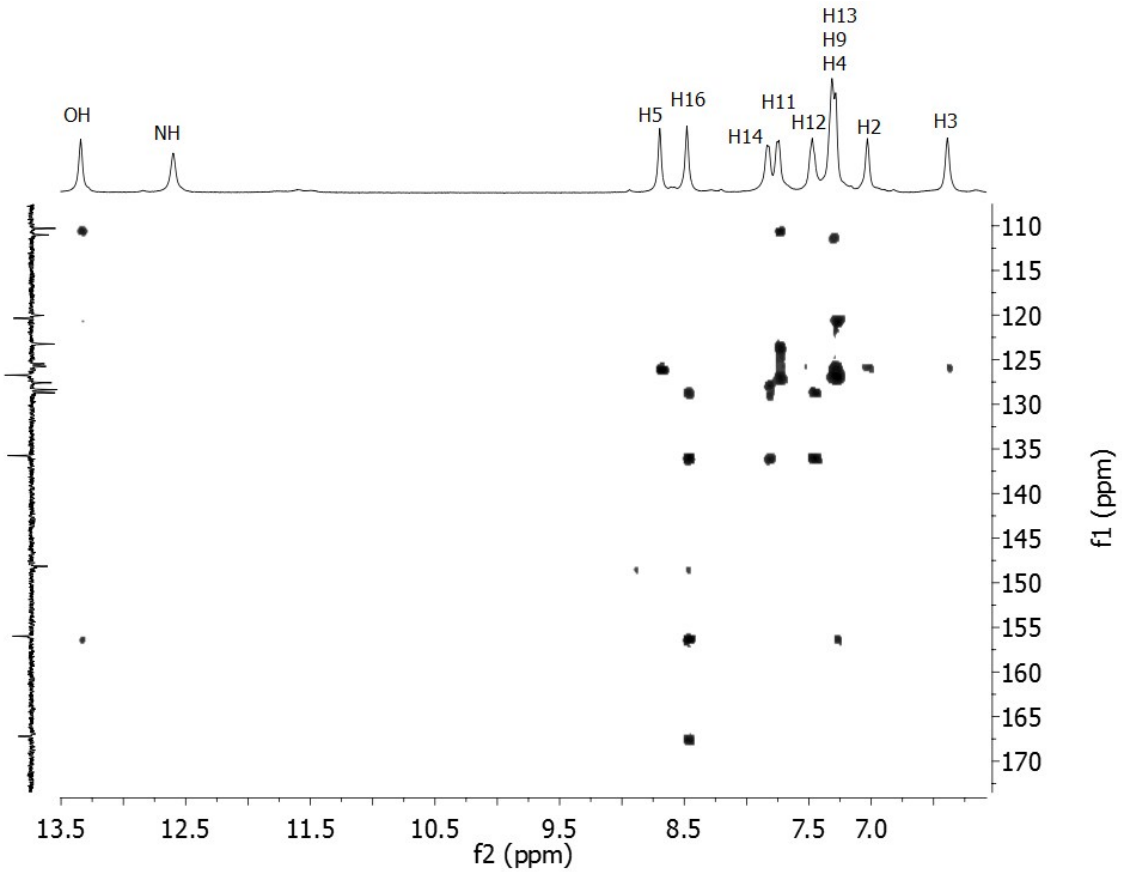

Figure S10 – HMBC correlation spectrum of $Zn(L^1)_2$, **7**, in DMSO-d_6 (chemical shifts in ppm, using TMS as internal reference).

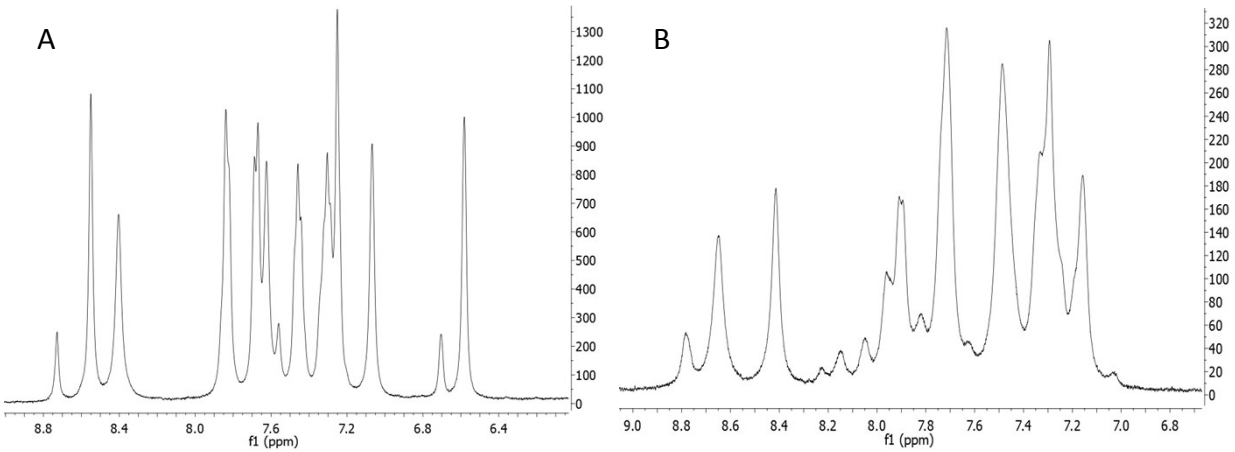

Figure S11 – (A) ^{1}H NMR spectrum of Zn(L^{2})$_2$ **8**, in MeOH-d_4 (chemical shifts in ppm, using TMS as internal reference). It is noted the presence of *ca.* 20 % free ligand in solution. (B) ^{1}H NMR spectrum of Zn(L^{3})$_2$ **9**, in DMSO-d_6 (chemical shifts in ppm, using TMS as internal reference). It is noted the presence of some free ligand in solution.

ESI 4 – Solution stability

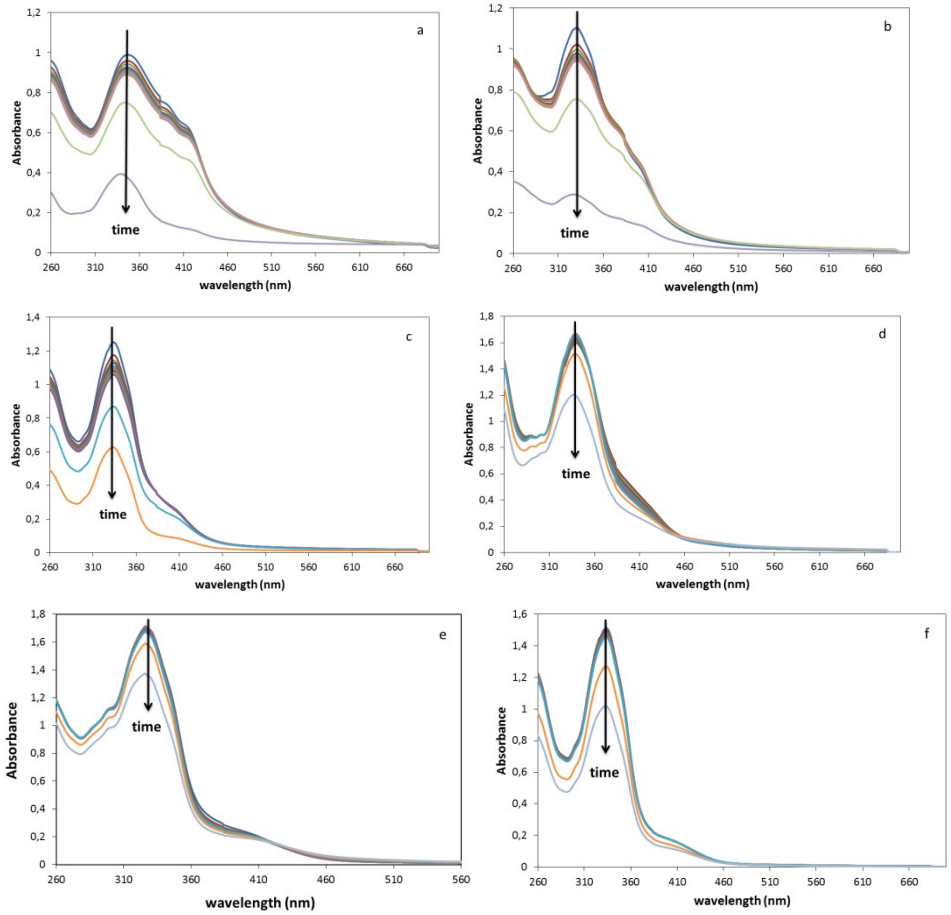

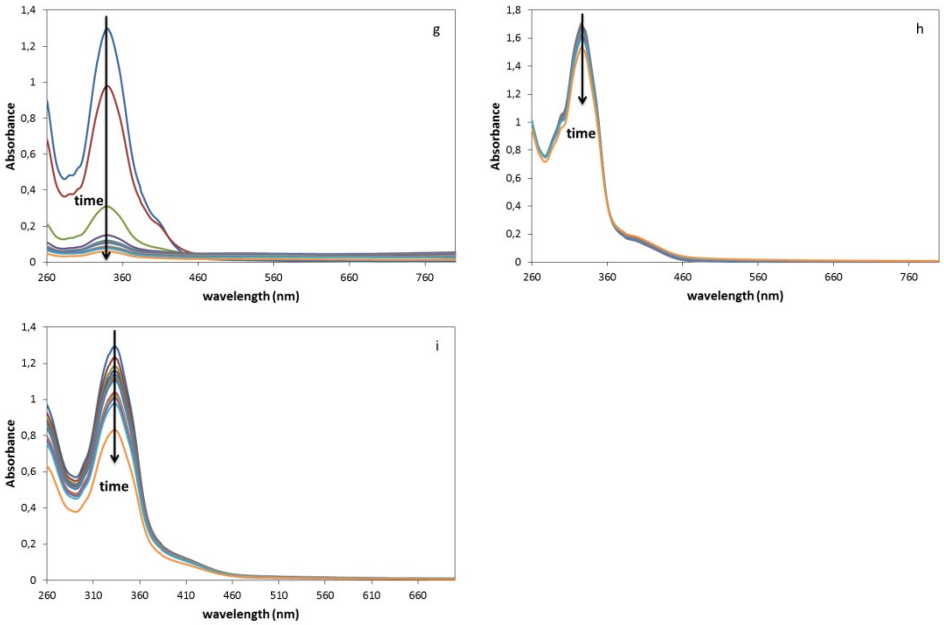

Figure S12 - UV-Vis absorption spectra measured during 24h for solutions in PBS buffer (pH 7.4 at 20°C) containing 20 - 30 μM of (a) **4** $Cu(L^1)_2$; (b) **5** $Cu(L^2)_2$; (c) **6** $Cu(L^3)_2$; (d) **1** $VO(L^1)_2$; (e) **2** $VO(L^2)_2$; (f) **3** $VO(L^3)_2$; (g) **7** $Zn(L^1)_2$; (h) **8** $Zn(L^2)_2$; and (i) **9** $Zn(L^3)_2$.

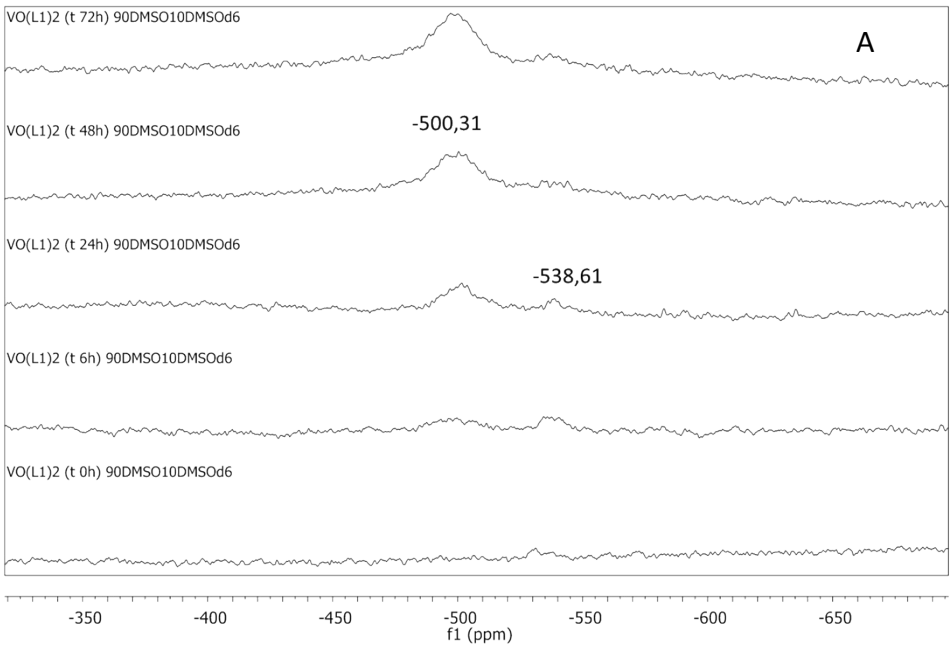

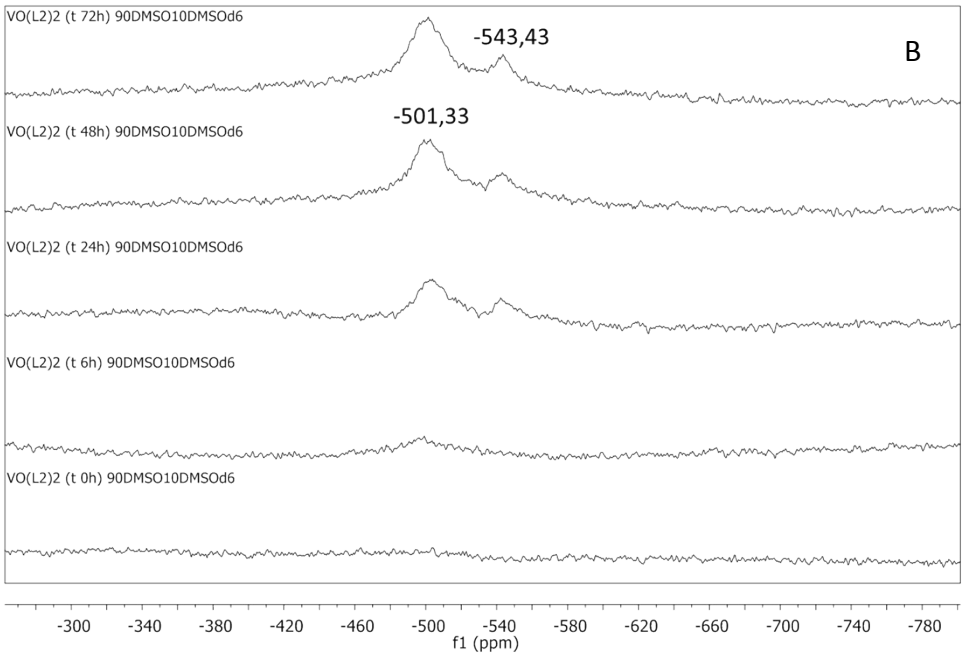

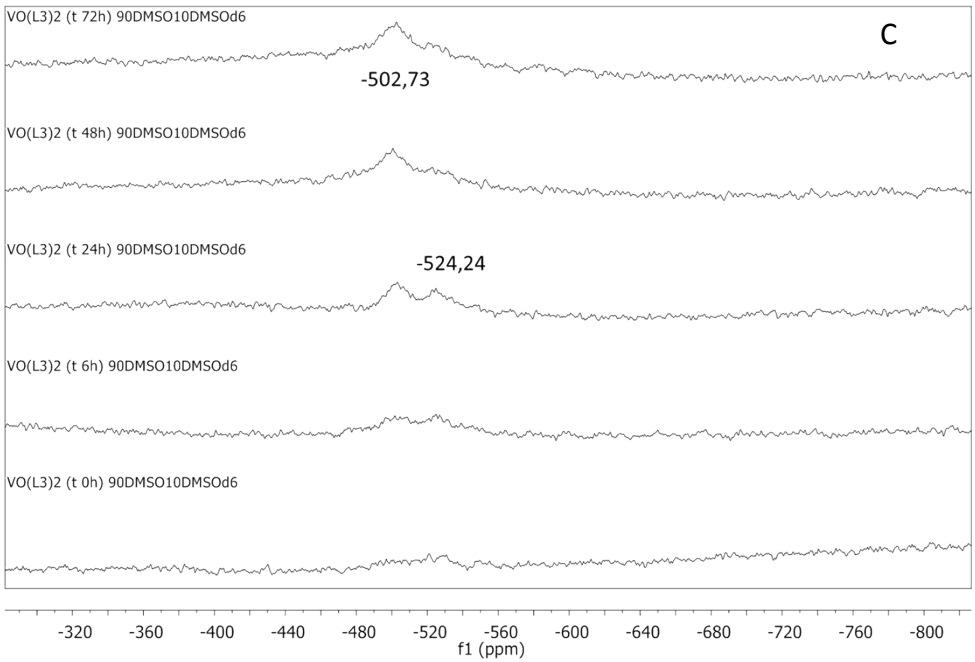

Figure S13 – ^{51}V NMR spectra measured during 72 h for solutions in DMSO with 10% DMSO-d_6 containing 3.5 mM of (a) $VO(L^1)_2$; (b) $VO(L^2)_2$; (c) $VO(L^3)_2$.

ESI 5 – Theoretical Calculations

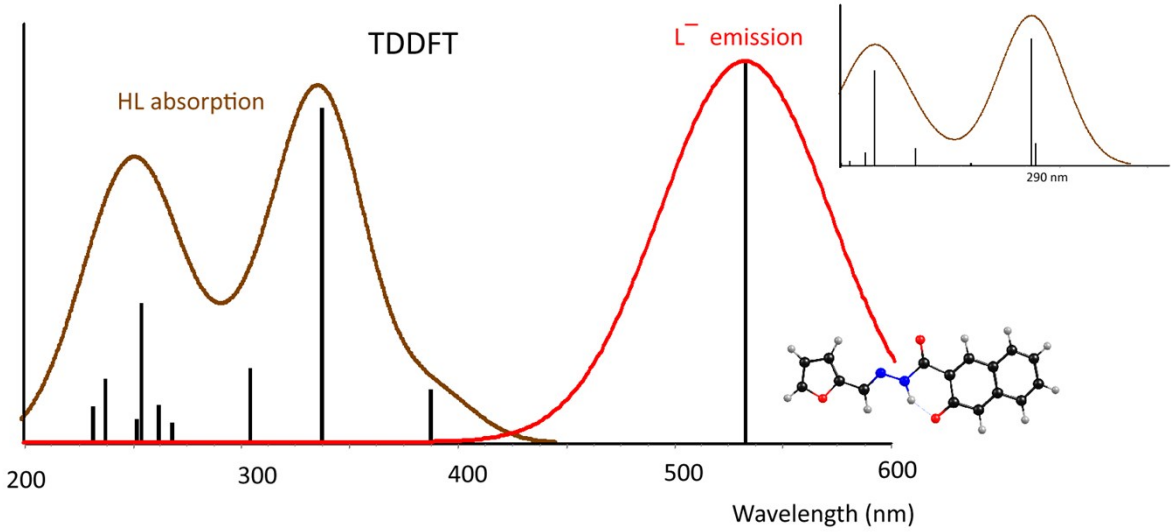

Figure S14 – TDDFT absorption (HL) and emission spectra. The band at 380 nm appears also in the experimental spectrum as a long Gaussian tail, absent in the simulated protonated species at the anionic geometry, see insert.

ESI 6 – Albumin binding

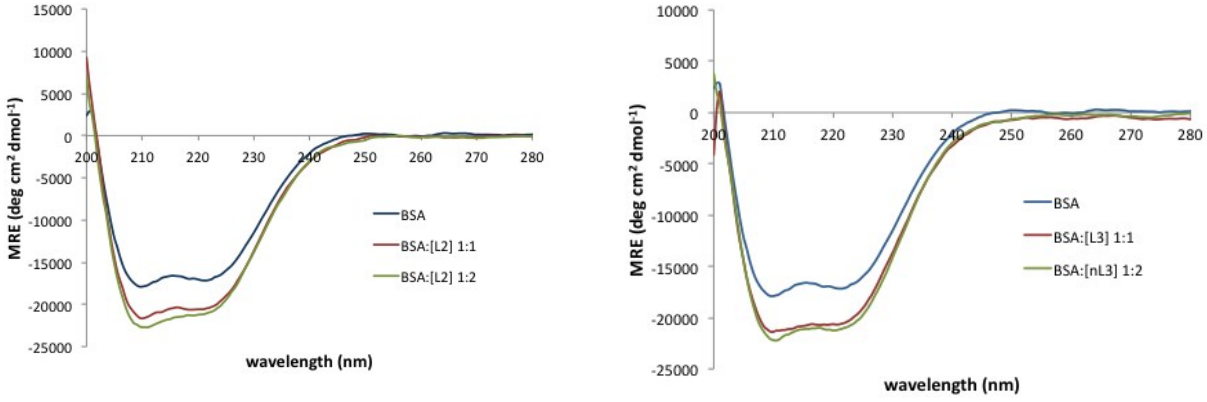

Figure S15 - Far-UV circular dichroism spectra measured for solutions containing BSA (*ca.* 1μM) and molar ratios of BSA:compound of 1 or 2 for HL^2 and HL^3. MRE is the mean residue elipticity.

Table S4 – Increase in the α-helical content of BSA calculated with equation 2 (at 208 nm), for BSA:compound ratios of 1:1 or 1:2.

Compound	**1:1**	**1:2**
HL^1	19	28
HL^2	12	16
HL^3	12	14
$VO(L^1)_2$ (**1**)	7	4
$VO(L^2)_2$ (**2**)	4	4
$VO(L^3)_2$ (**3**)	3	8
$Cu(L^1)_2$ (**4**)	2	2
$Cu(L^2)_2$ (**5**)	3	3
$Cu(L^3)_2$ (**6**)	5	5
$Zn(L^1)_2$ (**7**)	3	5
$Zn(L^2)_2$ (**8**)	4	4
$Zn(L^3)_2$ (**9**)	6	5

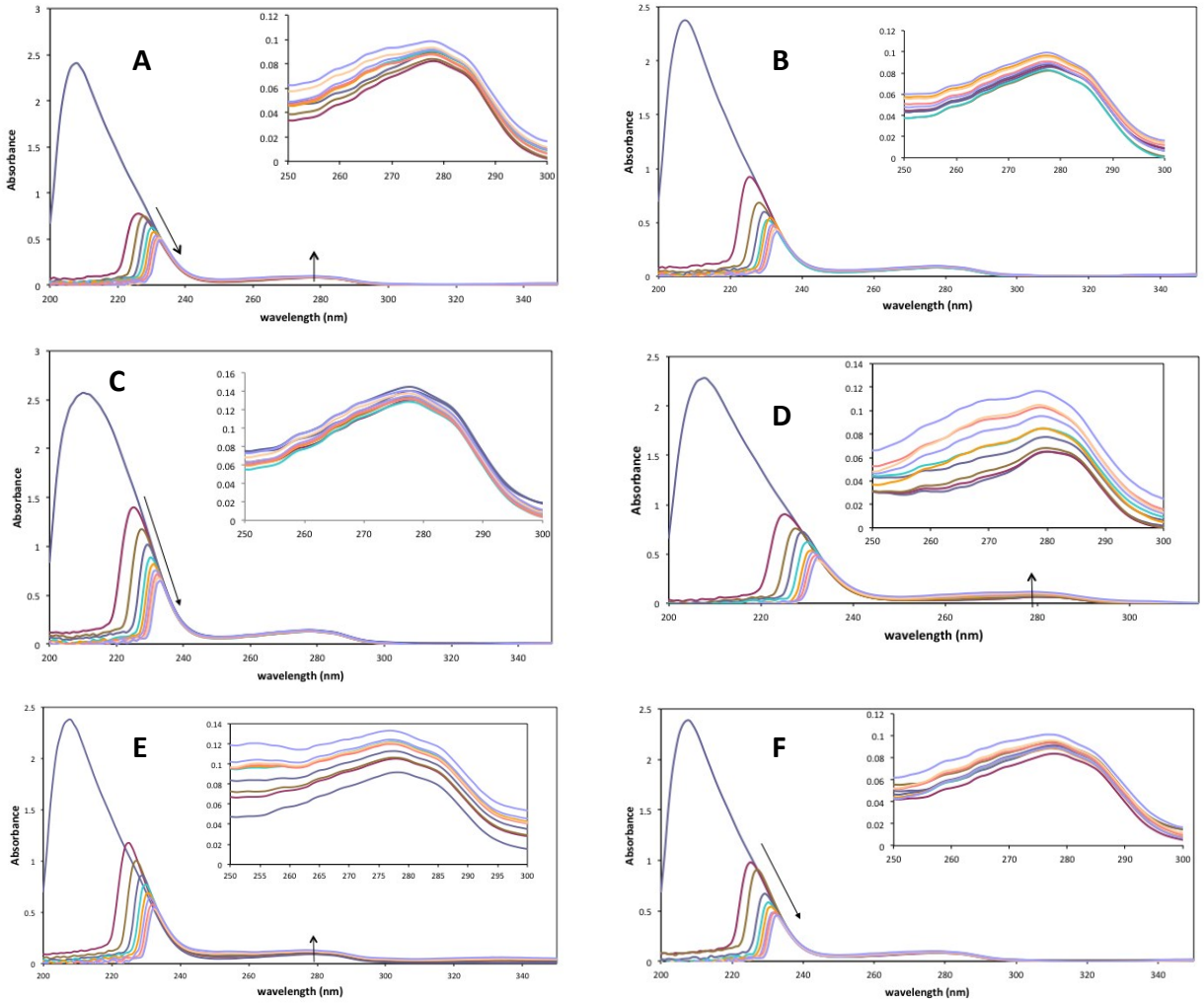

Figure S16 - UV absorption spectra measured for solutions containing BSA (*ca.* 3μM) and molar ratios of compound:BSA from 0 to 4. A) HL^1, B) HL^2, C) HL^3, D) **1**, E) **2** and F) **3.**

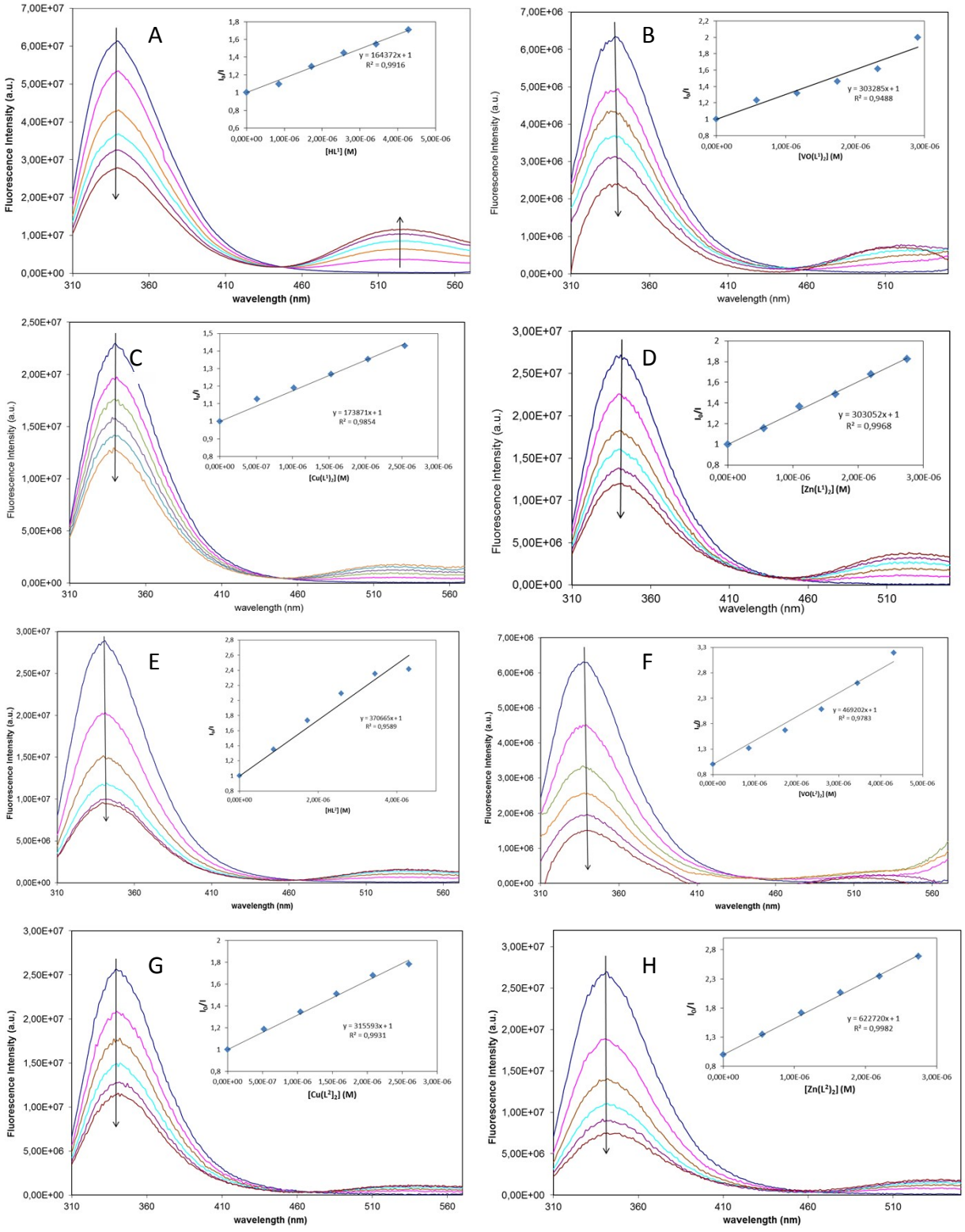
A
Fluorescence Intensity (a.u.)
wavelength (nm)
y = 164372x + 1
R² = 0,9916
[HL¹] (M)
B
y = 303285x + 1
R² = 0,9488
[VO(L¹)₂] (M)
C
y = 173871x + 1
R² = 0,9854
[Cu(L¹)₂] (M)
D
y = 303052x + 1
R² = 0,9968
[Zn(L¹)₂] (M)
E
y = 370665x + 1
R² = 0,9589
[HL²] (M)
F
y = 469202x + 1
R² = 0,9783
[VO(L²)₂] (M)
G
y = 315593x + 1
R² = 0,9931
[Cu(L²)₂] (M)
H
y = 622720x + 1
R² = 0,9982
[Zn(L²)₂] (M)

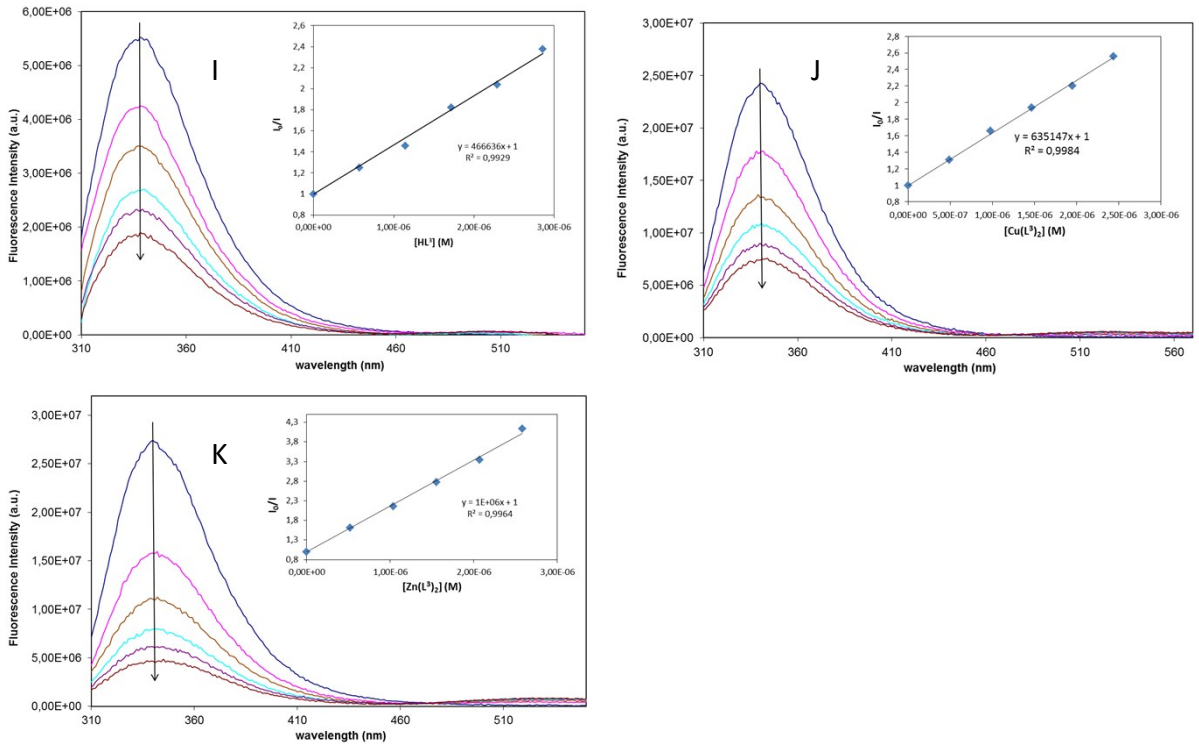

Figure S17 – Steady-state fluorescence quenching experiments for solutions containing BSA (*ca.* 1.5μM) and molar ratios of compound:BSA from 0 to 2 in 0.3% DMSO/ PBS aqueous buffer pH 7.4 after subtraction of blank emission spectra (arrows indicate the variation observed with increasing concentration of the compound). Insets: Stern-Volmer plots at emission maxima (I_0/I) obtained from the measurements (I_0/I data were corrected for inner-filter-effects). A) HL^1, B) **1**, C) **4**, D) **7**, E) HL^2, F) **2**, G) **5**, H) **8**, I) HL^3, J) **6** and K) **9**.

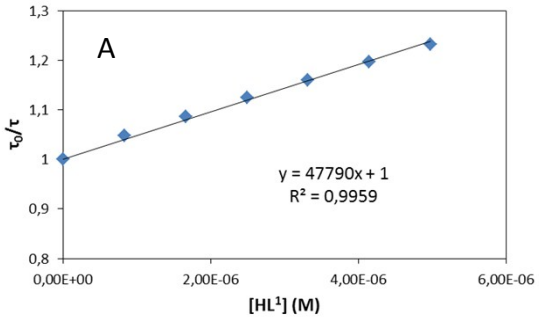
A
y = 47790x + 1
R² = 0,9959
τ0/τ
[HL1] (M)

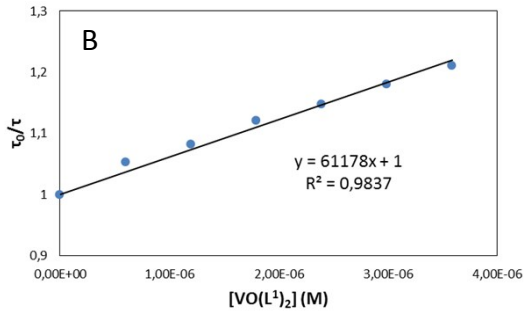
B
y = 61178x + 1
R² = 0,9837
τ0/τ
[VO(L1)2] (M)

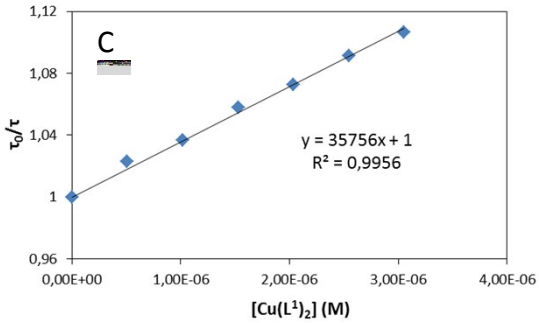
C
y = 35756x + 1
R² = 0,9956
τ0/τ
[Cu(L1)2] (M)

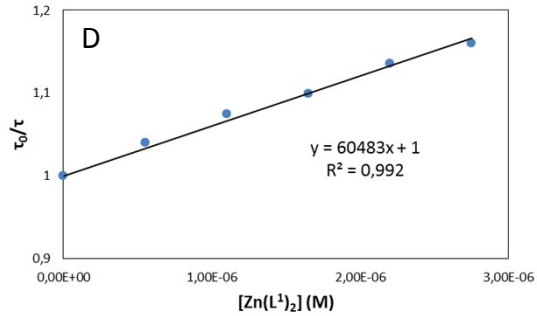
D
y = 60483x + 1
R² = 0,992
τ0/τ
[Zn(L1)2] (M)

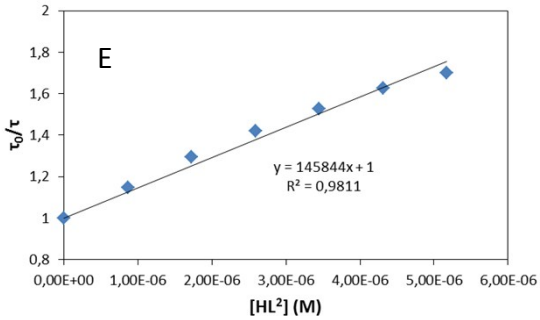
E
y = 145844x + 1
R² = 0,9811
τ0/τ
[HL2] (M)

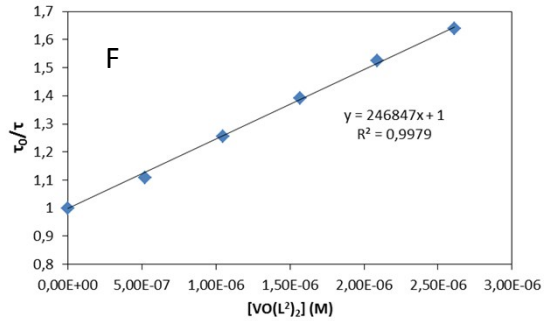
F
y = 246847x + 1
R² = 0,9979
τ0/τ
[VO(L2)2] (M)

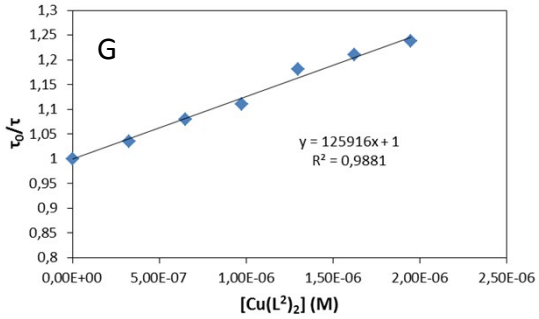
G
y = 125916x + 1
R² = 0,9881
τ0/τ
[Cu(L2)2] (M)

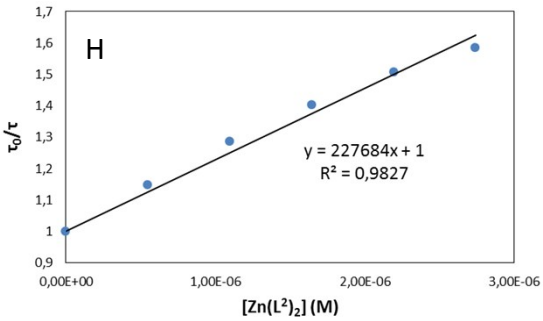
H
y = 227684x + 1
R² = 0,9827
τ0/τ
[Zn(L2)2] (M)

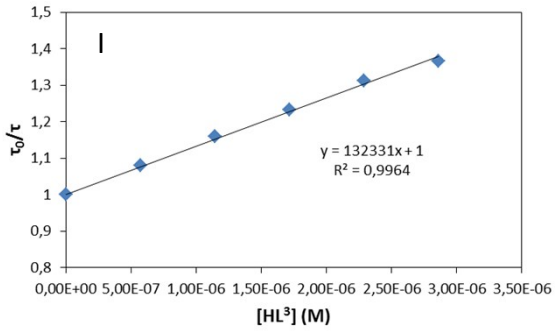
I
y = 132331x + 1
R² = 0,9964
τ0/τ
[HL3] (M)

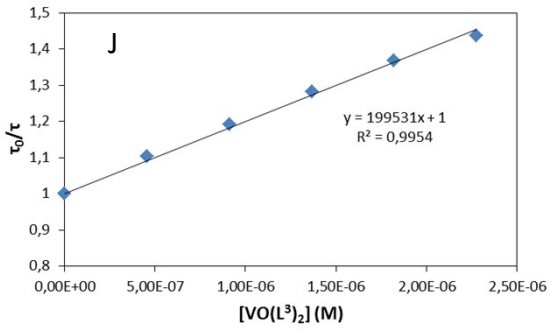
J
y = 199531x + 1
R² = 0,9954
τ0/τ
[VO(L3)2] (M)

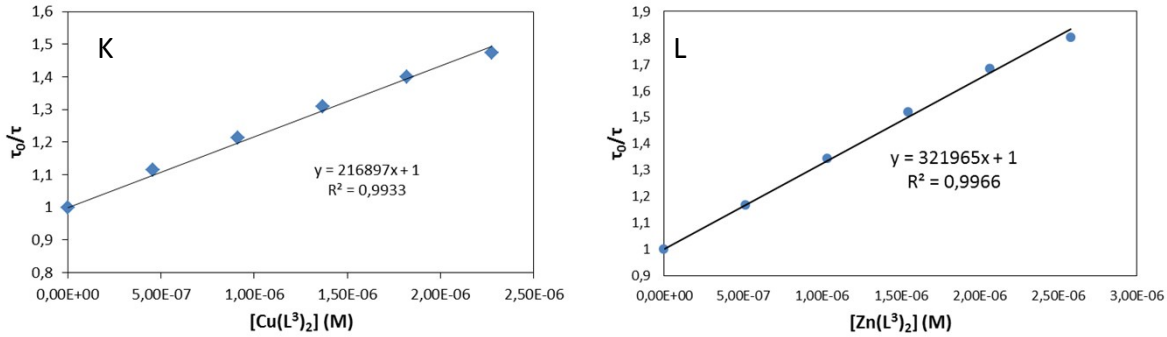

Figure S18 – Stern-Volmer plots obtained from the measurements of time-resolved fluorescence quenching experiments (τ_0/τ) for solutions containing BSA (*ca.* 1.5 μM) and molar ratios of compound:BSA from 0 to 2 in 0.3% DMSO/ PBS aqueous buffer pH 7.4. A) HL^1, B) **1**, C) **4**, D) **7**, E) HL^2, F) **2**, G) **5**, H) **8**, I) HL^3, J) **3**, K) **6** and L) **9**.

Table S5 - BSA fluorescence time-resolved quenching experimental results after analysis with the Stern-Volmer equations.

	K_{SV} (M^{-1})
HL^1	4.78×10^4
1	6.12×10^4
4	3.68×10^4
7	6.05×10^4
HL^2	1.46×10^5
2	4.27×10^5
5	1.26×10^5
8	2.28×10^5
HL^3	1.32×10^5
3	2.00×10^5
6	2.17×10^5
9	3.22×10^6

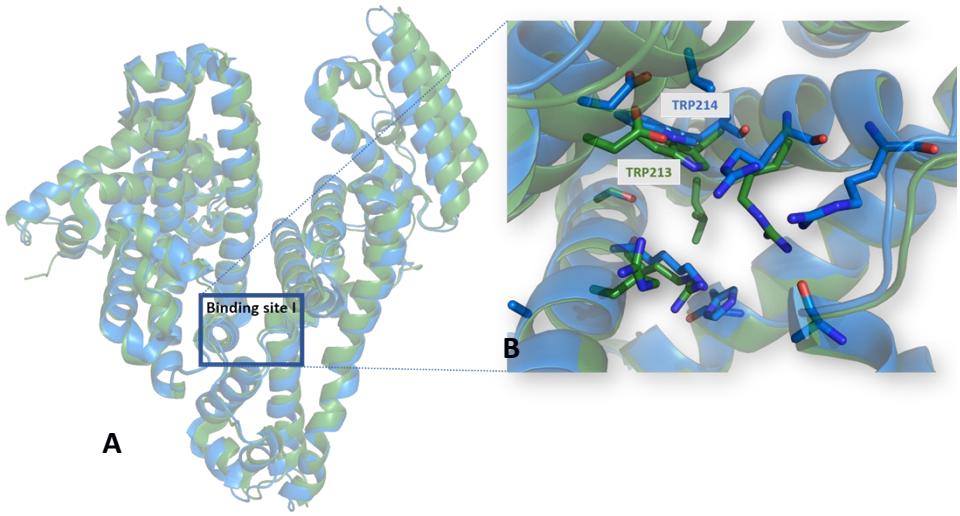

Figure S19 – **(A)** Superimposed chains of Bovine Serum Albumin and Human Serum Albumin. BSA (PDB-ID:4JK4-A) is represented in green and HSA (PDB-ID:3LU6-A) represented in blue. **(B)** Zoom of binding site I, of sub-domain IIA for BSA (green) and HSA (blue), superimposed. The amino acids represented in sticks are the most relevant for interactions with the ligands.

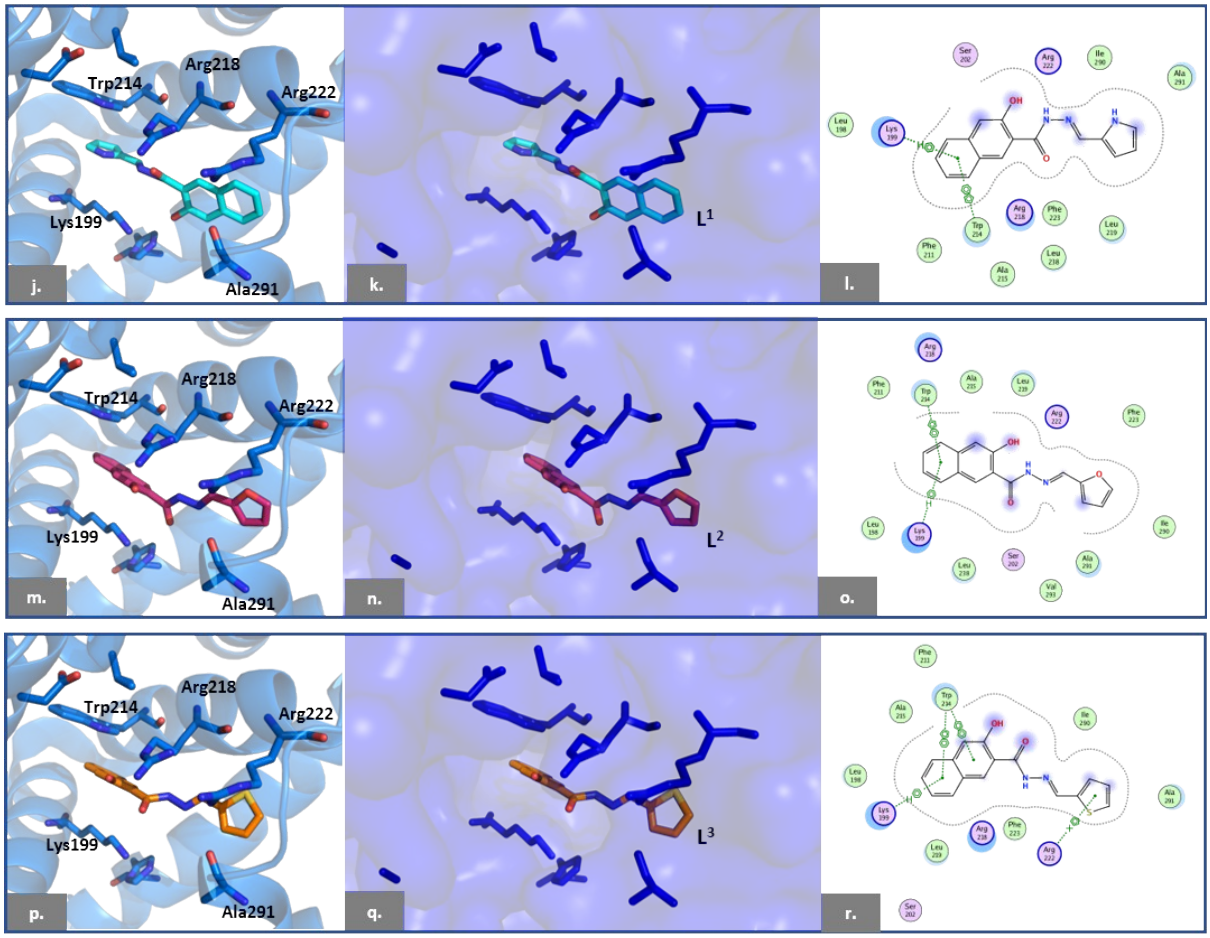

Figure S20 - Docking binding modes for HSA (PDB-ID: 3LU6).

HL^1- j. amino acid interaction of HL^1 inside the pocket. It is observed a stacking with Trp 213; **k.** surface view of 3LU6 binding pocket, with most important amino acid highlighted and HL^1 pose; **l.** 2D depiction of interactions of HL^1 inside HSA pocket.

HL^2- m. amino acid interaction of HL^2 inside the pocket. It is observed a stacking with Trp 213; **n.** surface view of 3LU6 binding pocket, with most important amino acid highlighted and HL^2 pose (more similar with L^3 pose); **o.** 2D depiction of interactions of HL^2 inside HSA pocket.

HL^3- p. amino acid interaction of HL^3 inside the pocket. It is observed a stacking with Trp 213; **q.** surface view of 3LU6 binding pocket, with most important amino acid highlighted and HL^3 pose; **r.** 2D depiction of interactions of HL^3 inside HSA pocket.

Table S6 - Validation of the system BSA's PDB-ID 4JK4 – interactions and distances observed between the crystallographic ligand and amino acids from the binding pocket

	Score	RMSD
Chemplp	50.84	0.5
Goldscore	56.33	0.5

	AA		interaction	Distance	Ligand
Crystallographic Ligand	Trp213	Crystal	Receptor exposure		
		CHEMPLP	Receptor exposure		
		GOLD	Receptor exposure		
	Arg194	Crystal	H-acceptor	2.93; 3.67	O
		CHEMPLP	H-acceptor ionic	2.95 2.95	O
		GOLD	H-acceptor ionic	2.59; 3.12; 3.16 2.59; 3.16; 3.76	O O
	Arg198	Crystal	H-acceptor ionic	3.21 2.43; 3.21; 3.45; 3.53	O O
		CHEMPLP	basic		
		GOLD	basic		
	Ser201	Crystal	H-donor	3.56	I
		CHEMPLP	polar		
		GOLD	-	-	-
	Ser214	Crystal	-	-	-
		CHEMPLP	H-donor	3.35	I
		GOLD	H-donor	3.12	I
	Arg217	Crystal	H-acceptor ionic	3.36 3.36; 3.84; 3.97	O O
		CHEMPLP	H-acceptor	3.85	I
		GOLD	H-acceptor	3.95	I
	Asp450	Crystal	H-donor	3.54	I
		CHEMPLP	-	-	-
		GOLD	-	-	-

Table S7 - Validation of the system HSA's PDB-ID 3UL6 – interactions and distances observed between crystallographic ligand and amino acids from binding pocket

	Score	RMSD
Chemplp	99.19	1.4
Goldscore	74.71	1.3

	AA		interaction	Distance	Ligand
Crystallographic Ligand	Trp214	Crystal	π-π	3.58	6-ring
		CHEMPLP		3.78	6-ring
		GOLD	π-π	3.58	6-ring
	Lys199	Crystal	Ionic π-H H-acceptor	3.19, 3.31 3.53; 3.79 3.19	O 5-ring; 6-ring O
		CHEMPLP	Ionic π-H H-acceptor	2.67; 2.74 3.61 2.67; 2.74	O 5-ring; 6-ring O
		GOLD	Ionic π-H H-acceptor	2.60; 3.09 3.64; 3.86 2.60; 2.09	O 5-ring; 6-ring O
	Arg218	Crystal	Receptor exposure		
		CHEMPLP	Receptor exposure		
		GOLD	Receptor exposure		
	His242	Crystal	H-acceptor	3.04	O
		CHEMPLP	H-acceptor	3.07	O
		GOLD	H-acceptor	2.85	O
	Ala291	Crystal	π-H	4.06	6-ring
		CHEMPLP	π-H	4.23	6-ring
		GOLD	-	-	-

Table S8 - Interactions between HL^1, HL^2 and HL^3 with BSA- 4JK4.

Aminoacid		Interaction	Distance
Trp213	HL^1	**π-π**	3.33; 3.53; 3.71; 3.73
	HL^2		2.96; 3.31; 3.60
	HL^3		3.13; 3.20; 3.46
Arg194	HL^1	Receptor exposure	-
	HL^2	H- acceptor	2.84
	HL^3		2.76
Arg198	HL^1	Basic	-
	HL^2	Receptor exposure, basic	-
	HL^3	H-acceptor	2.92
Ser201	HL^1	H-donor	3.45
	HL^2	Polar	
	HL^3		-
Ala209	HL^1	Lipophilic	-
	HL^2	-	-
	HL^3	-	-
Leu210	HL^1	Lipophilic	-
	HL^2		-
	HL^3		-
Arg217	HL^1	-	-
	HL^2	Receptor exposure	-
	HL^3		-

Table S9- Interactions between L^1, L^2 and L^3 with HSA- 3LU6

Aminoacid		Interaction	Distance
Trp214	HL^1	**π-π**	3.79
	HL^2		3.75
	HL^3		3.49; 3.99
Lys199	HL^1	π-H	-
	HL^2		3.83
	HL^3		3.96
Arg218	HL^1	Receptor exposure	-
	HL^2		-
	HL^3		-
Ala291	HL^1	π-H	4.19
	HL^2	Receptor exposure	-
	HL^3		-
Arg222	HL^1	Polar	-
	HL^2		-
	HL^3	π- cation	3.76

Table S10 - Score values obtained with Goldscore fitness function for BSA (PDB-ID 4JK4) and HAS (PDB-ID 3UL6)

		Score	S(hb_ext)	S(vdw_ext)	S(hb_int)	S(int)	intcor
HL^1	BSA	**65.47**	1.92	46.88	0.00	-0.91	-4.30
	HSA	**62.66**	6.04	41.63	0.00	-0.62	-4.30
HL^2	BSA	**64.48**	6.06	44.57	0.00	-2.87	-4.44
	HSA	**65.37**	11.35	40.33	0.00	-1.42	-4.43
HL^3	BSA	**66.62**	6.00	45.85	0.00	-2.43	-4.37
	HSA	**64.73**	5.88	44.24	0.00	-1.97	-4.36
$VO(L^2)_2$	BSA	**61.66**	0.00	44.96	0.00	-0.16	-3.42
	HSA	**56.24**	5.85	36.70	0.00	-0.08	-3.42
$Cu(L^2)_2$	BSA	**67.73**	0.92	48.82	0.00	-0.32	-3.35
	HSA	**68.61**	0.00	50.27	0.00	-0.50	-3.35
$Zn(L^2)_2$	BSA	**58.88**	0.00	42.85	0.00	-0.04	-3.72
	HSA	**71.46**	4.25	49.58	0.00	-0.96	-3.72

Table S11 - Interactions between L^2 complexes and BSA- (PDB-ID 4JK4).

Aminoacid		Interaction	Distance
Trp213	$VO(L^2)_2$	Receptor exposure	
	$Cu(L_2)_2$		
	$Zn(L_2)_2$		
Arg194	$VO(L^2)_2$	Receptor exposure	
	$Cu(L_2)_2$		
	$Zn(L_2)_2$		
Lys294	$VO(L^2)_2$	-	
	$Cu(L_2)_2$	H-acceptor	3.16
	$Zn(L_2)_2$	Receptor exposure	
Pro338	$VO(L^2)_2$	-	
	$Cu(L_2)_2$	H-donor	2.56
	$Zn(L_2)_2$	Receptor exposure	

Table S12 - Interactions between L^2 complexes and HSA- 3LU6

Aminoacid		Interaction	Distance
Trp214	$VO(L^2)_2$	π-π	3.58
	$Cu(L_2)_2$	π-π	3.11
	$Zn(L_2)_2$	-	
Lys 199	$VO(L^2)_2$	π-H	3.53
	$Cu(L_2)_2$	Ligand exposure	
	$Zn(L_2)_2$	Ligand exposure	
Arg 218	$VO(L^2)_2$	-	
	$Cu(L_2)_2$	H- acceptor	3.48
	$Zn(L_2)_2$	-	
His 242	$VO(L^2)_2$	H-acceptor	2.98; 3.04
	$Cu(L_2)_2$	-	
	$Zn(L_2)_2$	-	
Tyr 452	$VO(L^2)_2$	-	
	$Cu(L_2)_2$	-	
	$Zn(L_2)_2$	π-π	3.4
Cys 488	$VO(L^2)_2$		
	$Cu(L_2)_2$		
	$Zn(L_2)_2$	H-donor	3.32

Table S13 – Metal force-fields .[2]

Metal	Acceptor	Force
V	N2DA	-10
V	O2A	-5
V	OCO2A	-15
V	N1A	-10
V	N3A	-10
V	O3A	-10
V	N2A	-10
V	N3DA	-10
V	O3DA	-1
V	NACIDA	-15
V	O2NA	-1
V	ONO2A	-10
V	SMIN	-20
V	SACC	-15
V	NARA	-20
V	O3MINUSA	-20
V	OMINUSA	-20
Cu	N2DA	-10
Cu	O2A	-5
Cu	OCO2A	-15
Cu	N1A	-10
Cu	N3A	-10
Cu	O3A	-10
Cu	N2A	-10
Cu	N3DA	-10
Cu	O3DA	0
Cu	NACIDA	-15
Cu	O2NA	-1
Cu	ONO2A	-10
Cu	SMIN	-15
Cu	SACC	-15
Cu	NARA	-20
Cu	O3MINUSA	-20
Cu	OMINUSA	-20
Zn	N2DA	-10
Zn	O2A	-5
Zn	OCO2A	-15
Zn	N1A	-10
Zn	N3A	-10
Zn	O3A	-10
Zn	N2A	-10
Zn	N3DA	-10
Zn	O3DA	0
Zn	NACIDA	-15
Zn	O2NA	-1
Zn	ONO2A	-10
Zn	SMIN	-15
Zn	SACC	-15
Zn	NARA	-20
Zn	O3MINUSA	-20
Zn	OMINUSA	-20

ESI7 – Toxicity

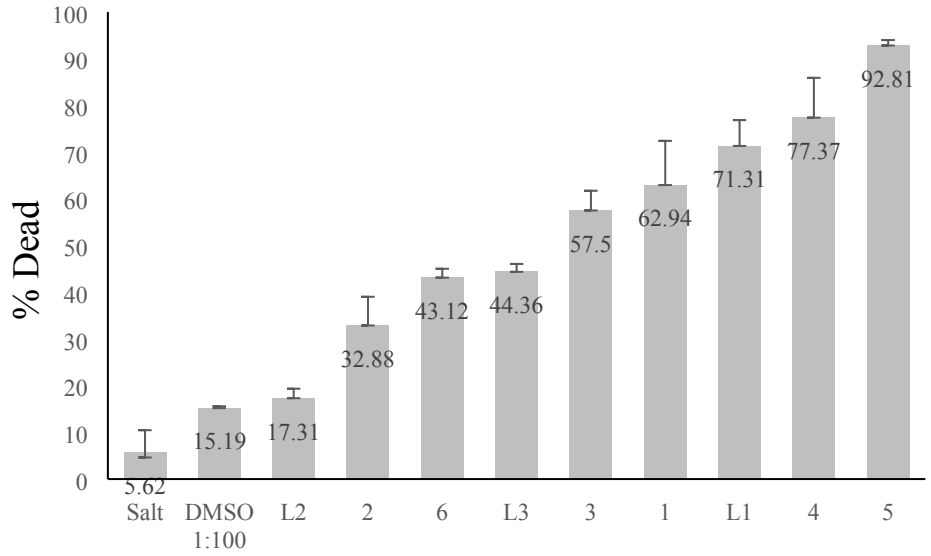

Figure S21 – General toxicity of the compounds, at 0.1 mg/mL using the *Artemia salina* assay.

References

1. F. H. Allen, *Acta Crystallogr B*, 2002, **58**, 380-388.
2. G. Sciortino, J. Rodrıguez-Guerra Pedregal, A. Lledos, E. Garribba, J.-D. Marechal., J. Comput. Chem. 2017, DOI: 10.1002/jcc.2508